Applied Nanoscience (2018) 8:137–153
https://doi.org/10.1007/s13204-018-0656-5

ORIGINAL ARTICLE

Antibacterial applications of α-Fe_2O_3/Co_3O_4 nanocomposites and study of their structural, optical, magnetic and cytotoxic characteristics

Mayank Bhushan[1] · Yogesh Kumar[2] · Latha Periyasamy[2] · Annamraju Kasi Viswanath[1]

Received: 21 September 2017 / Accepted: 5 January 2018 / Published online: 5 February 2018

Abstract
Owing to their multiple mechanisms of bactericidal activity, inorganic metal oxides and hybrid metal oxide nanocomposites may serve as a new class of effective disinfectants. Among metal oxide nanoparticles, iron oxide nanoparticles exhibit minimal or no cytotoxicity to human cells with very efficient bactericidal properties over a wide spectrum of bacteria. This paper presents the very first report on antibacterial properties of novel nanocomposites of iron oxide and cobalt oxide nanoparticles against pathogenic bacterial strains *B. subtilis*, *S. aureus*, *E.coli* and *S. typhi*. The enhanced bactericidal activity of the Fe/Co oxide nanocomposite was the result of synergistic effect of iron oxide and cobalt oxide nanoparticles. The nanocomposites were synthesized using co-precipitation route with increasing cobalt content in the sample and further characterized using XRD, TEM, Raman and VSM to investigate structural, optical and magnetic properties of the prepared nanocomposites, respectively. Also, the prepared nanocomposites were highly biocompatible and found non-toxic to human cell line MCF7.

Keywords α-Fe_2O_3 · Co_3O_4 · Nanocomposite · Antibacterial · Ferromagnetic

Introduction

Bactericidal behavior is attributed to the compounds that restrictedly eradicate bacteria or hamper their growth without causing harm to surrounding cells and tissues. Most of the currently used antibiotics like penicillins, cephalosporins or carbapenems are chemically modified natural compounds such as β-lactams. Antibiotics with pure natural origin like aminoglycosides and pure synthetic product like sulfonamides are also in use (Nussbaum et al. 2006). These conventional antibiotics are organic moieties of low molecular weights and are the backbone to fight contagious diseases. However, the broad use and abuse of antibiotics have resulted in emergence of bacterial resistance through evolutionary processes (Levy and Marshall 2004; Jayaraman 2009; Chambers and DeLeo 2009; Huh and Kwon 2011; Zhang et al. 2011; Moritz and Geszke-Moritz 2013). This demands an unconventional and new approach to combat pathogenic bacteria and should have the potential to trespass bacterial resistance (Blecher et al. 2011; Pelgrift and Friedman 2013). Among all the new strategies, use of nanoscale materials has emerged as most promising alternative of traditional antibiotics with very distinct pathways of bactericidal action. Other than their use as an antibiotic to combat contagious diseases, antibacterial agents have diverse applications in food processing and as coating agents on medical devices and implants to make them resistant against microbial infections. So, for this purpose the main advantages of using inorganic antibacterial agents over the traditionally used organic ones are their much higher stability at elevated temperatures and pressures with no loss of medicinal property (Xia 2008; Hajipour et al. 2012; Hood and Skaar 2012; Aruguete et al. 2013; Chipara et al. 2015). For this application, different forms of inorganic nanomaterials like

✉ Annamraju Kasi Viswanath
v_kasi@hotmail.com

Mayank Bhushan
mayankbhushan1984@gmail.com

Yogesh Kumar
yogeshkumarbiotech@gmail.com

Latha Periyasamy
lathaperiyasamy6@gmail.com

[1] Centre for Nanoscience and Technology, Pondicherry University, Puducherry 605014, India

[2] Department of Biochemistry and Molecular Biology, Pondicherry University, Puducherry 605014, India

powders, organic/inorganic hybrid coatings, powders coated on cellulose fabric, etc. can be used and they were quite successful in neutralizing a vast range of Gram-positive and Gram-negative bacteria (Foster et al. 2011).

Recently, there was growing interest in fabricating colloid metal and metal oxide nanoparticles of bactericidal functionality against which pathogens have not yet develop resistance. These colloid nanoparticles with antibacterial properties can be used to combat bacterial pathogens because of their high bactericidal activity at very low particle concentrations (Davies and Davies 2010). The antimicrobial properties of nanomaterials are attributed to their particle size, morphology and unique catalytic, photoactive, optical and thermal properties (Liu et al. 2009; Brayner et al. 2010; Zhang et al. 2010). Different metal oxide nanoparticles with bactericidal property have varying mechanisms of action against bacterial cells (Fu et al. 2005; Makhluf et al. 2005; Parham et al. 2016). Although the magnetite (Fe_3O_4) and maghemite ($^{\gamma}$-Fe_2O_3) are known to exhibit antibacterial properties (Kong et al. 2010; Tran et al. 2010; Chen et al. 2012), there are not many reports on antibacterial properties of hematite (α-Fe_2O_3) nanocrystals in the past. Recently, hematite nanocrystals have attracted scientific attention for antibacterial application after it has been approved by the Food and Drug Administration (FDA) for food and medical applications (Basnet et al. 2013; Arakha et al. 2015; Rafi et al. 2015; Nor et al. 2016; Rudramurthy et al. 2016; Rufus et al. 2016; Sharma et al. 2016; Stankic et al. 2016). Other advantages of using hematite nanocrystals are their high chemical stability in varying pH range, biocompatibility and low manufacturing cost (Cesar et al. 2006). The bactericidal activity of iron oxide nanoparticles is due to the generation of oxygen-free radicals upon conversion of hydrogen peroxide into highly reactive hydroxyl radicals via Fenton reaction (Touati 2000). These free radicals act in multiple ways like depolymerization of polysaccharides, breaking of DNA strands, inactivation of enzymes and peroxidation of membrane lipids, which ultimately results in death of bacteria (Weinberg 1999; Touati 2000; Kohanski et al. 2007; Pareta et al. 2008). The antibacterial behavior of cobalt oxide nanoparticles is known but there are very few reports which detail the underlying mechanisms of their bactericidal action. The general understanding is that, in the presence of an aqueous medium, i.e., inside the bacterial cell, the cobalt oxide nanoparticles trigger the production of reactive oxygen species (ROS). These ROS disintegrate all the structural building blocks of bacterial cells, i.e., carbohydrates, proteins and lipids by interacting with them which eventually cause death of bacteria. They also interact with the genetic material of bacteria and interrupt DNA replication, transcription and protein synthesis which lead to bacterial death (Wang et al. 2010; Dasari et al. 2013; Ghosh et al. 2014; Khan et al. 2015).

In the present work, we report the detailed investigations of in vitro antibacterial activities of α-Fe_2O_3/Co_3O_4 nanocomposites against four pathogenic bacteria *B. subtilis*, *S. aureus*, *E.coli* and *S. typhi*. The nanocomposites were synthesized using cost-effective wet-chemical approach and further characterized to study the structural, morphological, optical and magnetic properties. To the best of our knowledge, the synergistic effect of magnetic nanocomposite of iron oxide and cobalt oxide as an antibacterial agent is not yet reported in the available literature and hence this study is carried out to mainly investigate the antibacterial properties of α-Fe_2O_3/Co_3O_4 composite nanoparticles. The simultaneous use of different mechanisms results in a situation where it is very unlikely for the bacterial cell to develop resistance to these nanoparticles because to do so, the bacteria have to go through multiple mutations simultaneously in a single cell which is a very rare event and almost impossible. Additionally, cytotoxicity of the prepared composite samples was evaluated via MTT assay and the prepared samples were found non-toxic to human cell line MCF7.

Materials and methods

Materials

Ferrous sulphate heptahydrate ($FeSO_4{\cdot}7H_2O$), cobalt nitrate hexahydrate [$Co(NO_3)_2{\cdot}6H_2O$] and sodium hydroxide were purchased from Sigma-Aldrich, India. Nutrient agar media, nutrient broth and ethanol were purchased from Hi-media, India. Streptomycin, gentamycin, penicillin, FBS (Fetal bovine serum), DMEM (Dulbecco's Modified Eagle's medium), MTT (methyl thiazolyl diphenyl-tetrazolium bromide), Triton X100, DMSO (Dimethyl sulfoxide), PBS (Phosphate-buffered saline) and 96-well tissue culture plates were purchased from Hi-Media, India. Double distilled water was used for all the experiments.

Synthesis of Fe/Co oxide nanocomposites and the pure samples of α-Fe_2O_3 and Co_3O_4 nanoparticles

Nanocomposites of hematite (α-Fe_2O_3) and cobalt oxide (Co_3O_4) were also synthesized using co-precipitation method. The molar concentration of $FeSO_4{\cdot}7H_2O$ was kept constant as 0.1 M and the molar concentrations of $Co(NO_3)_2{\cdot}6H_2O$ were varied as 0.025, 0.05, 0.075 and 0.1 M, respectively. For synthesizing nanocomposites, first of all the required amounts of metal precursors were dissolved in 100 ml of double distilled water in a beaker and stirred for 10 min using magnetic stirrer allowing homogeneous mixing of the precursors in water. Following this, the above solution was titrated by dropwise addition of 0.8 M

(100 ml) NaOH solution under vigorous stirring. After 10 h of continuous stirring, the final products were collected by washing the prepared solutions thrice with double distilled water and once with ethanol using ultracentrifugation operated at 8000 rpm for 10 min. The obtained powder samples were calcined at 700 °C for 3 h and used as such for further characterizations. In a similar way, pure samples of α-Fe_2O_3 and Co_3O_4 were also prepared for comparison. Composition and code of all the prepared samples are tabulated in Table 1.

Characterization

Structural, morphological and elemental analysis of the prepared samples were carried out using XRD (X-ray diffractometer, model RigakuUltima IV with Cu K_α radiation 1.5418 Å, operating voltage 40 kV, current 40 mA and step size 0.02° in 2θ scan), and TEM (JEM2100) equipped with energy dispersive spectroscope (EDS). Optical studies of the prepared samples were carried out using confocal Raman spectrophotometer to re-conform the phase of nanomaterials by exciting them with Ar^+ laser 514 nm lines. Room temperature magnetic behavior of the samples was recorded using vibrating sample magnetometer, model VSMLake Shore 7404. Standard protocols were followed while performing all the above characterizations.

Antibacterial activity of α-Fe_2O_3/Co_3O_4 Nanocomposites

The antibacterial activities of Fe/Co oxide composite nanoparticles were investigated against two Gram-positive bacteria (*B. subtilis*, *S. aureus*) and two Gram-negative bacteria (*E.coli*, *S. typhi*) in triplicates by disc diffusion method and growth curve analysis method, respectively.

In Bauer–Kirby disc diffusion method (Bauer et al. 1966), molten Mueller–Hinton agar was poured into petri plates and allowed to solidify. Following this, the plates were inoculated with the overnight grown cultures of the above-mentioned bacteria. Autoclaved Whatman filter paper disks of 6 mm diameter were placed on the solidified agar and 20, 30 and 40 µl of nanoparticles suspension of each sample were loaded on the paper discs from their respective stock solutions (20 mg/ml). Double distilled water was used as suspension medium while preparing stock solution. Commercial antibiotic Gentamycin was used as a positive control and discs loaded with double distilled water served as negative/solvent control. Zone of inhibition was measured around each disc using antibiotic zone scale (Hi-media) after 24 h incubation of all the petri plates at 37 ± 1 °C.

Growth curve analysis was performed by inoculating fresh bacterial colonies in 100 ml of nutrient broth media in different flasks containing different concentrations (45, 60, 75, 90 and 120 mg/dl, respectively) of the FeK1, FeK4, Co_3O_4 and α-Fe_2O_3 nanoparticles. All the flasks inoculated with bacterial cultures were transferred on a shaker rotating with 200 rpm and incubated at 37 ± 1 °C. Bacterial growth in the nutrient broth media was measured by taking optical density (OD) of the bacterial suspension at 600 nm wavelength using UV–visible spectroscopy at fixed time intervals for 24 h. The flask containing bacterial culture alone (without nanoparticle) served as a positive control and used to evaluate the inhibitory effect of different concentrations of nanoparticles on bacterial growth. Bacterial growth curve was plotted by plotting a graph between OD and incubation time.

Table 1 Sample code and composition

S. no.	Sample description	Sample code
1.	α-Fe_2O_3	α-Fe_2O_3
2.	Co_3O_4	Co_3O_4
3.	0.1(M) Fe_2O_3 + 0.025(M) Co_3O_4	FeK1
4.	0.1(M) Fe_2O_3 + 0.05(M) Co_3O_4	FeK2
5.	0.1(M) Fe_2O_3 + 0.075(M) Co_3O_4	FeK3
6.	0.1(M) Fe_2O_3 + 0.1(M) Co_3O_4	FeK4

Cytotoxicity of α-Fe_2O_3/Co_3O_4 nanocomposites

The cell viability was quantified by performing MTT assay which measures in vitro cytotoxicity and cell proliferation. The MTT assay is a colorimetric assay which upon cleavage by viable cell's mitochondrial enzyme succinate-dehydrogenase yields a blue colored product formazan. The scanning multiwall spectrophotometer is used to read the amount of formazan crystals produced, which is proportional to the number of viable cells present (Mosmann 1983; Denizot and Lang 1986; Wan et al. 1994). The breast cancer cell line MCF7 cells were obtained from the National Center for Cell Sciences, Pune, India. The cells were cultured in Dulbecco's modified Eagle's medium (DMEM) supplemented with 10% fetal bovine serum (FBS), 100 IU/ml penicillin and 10 µg/ml streptomycin. The cell culture medium was maintained at 37 °C in 5% CO_2 environment. The cells were trypsinized and seeded (10×10^3 cells/well) in a 96-well tissue culture plate for 24 h. Following that, the old culture media were replaced with new one containing different concentrations of prepared nanoparticles. The tested concentrations were 50, 100, 200, 400, 600, 800, 1000 and 1600 µg/ml. Culture medium without nanoparticles was used as a negative control and the cells incubated with 1% Triton X100 were served as positive control. Each sample was kept in three wells to get statistically reliable results. After 24 h, the medium from each well was discarded and the cells were rinsed with 200 µl PBS followed by the addition of 10 µl of

the MTT stock solution (5 mg/ml) in each well. The medium was removed after 2 h incubation and the formazan crystals were solubilized in 100 µl of DMSO. The optical density of each well, which quantifies the number of viable cells, was read at 570 nm using an ELISA microplate reader (Molecular Devices, LLC, Sunnyvale, CA, USA).

Results and discussion

XRD

The X-ray diffraction patterns of Fe/Co oxide nanocomposites (FeK3 and FeK4) are shown in Fig. 1. Both the composite oxide samples exhibit the diffraction peaks of the cubic phase Co_3O_4 (JCPDS no.: 76-1802) and hexagonal phase α-Fe_2O_3 (JCPDS no.: 33-0664). Diffraction peaks due to the presence of any secondary phases such as cobalt–ferrite were not observed. This suggests that the prepared nanocomposites were composed of only α-Fe_2O_3 and Co_3O_4 and were highly pure. The average crystallite size of the sample FeK4 was estimated using Scherrer's formula and was found as 25.34 nm.

TEM

The high-resolution transmission electron micrographs of Fe/Co oxide nanocomposite (sample FeK4) are shown in Fig. 2a–h. The composite sample is a mix of rod shaped and roughly hexagonal shaped nanoparticles, as can be seen in Fig. 2a–c, e. Figure 2d shows the selected area diffraction (SAED) patterns of the nanorod shown in Fig. 2c. The SAED patterns suggest that the nanorod shown in Fig. 2c is superimposed on another nanorod and is single crystalline. Figure 2f shows the SAED patterns of hexagonal nanoparticle shown in Fig. 2e. The SAED patterns suggest that the hexagonal nanoparticle is crystalline and made up of nanocrystals oriented in a single plane. Figure 2g shows the zoomed in image of upper edge of hexagonal nanoparticle of Fig. 2e. The high-resolution TEM image shown in Fig. 2h was taken by focusing the electron beam on the junction site of light and dark shades of the particle shown in Fig. 2g, consisting of both iron oxide and cobalt oxide and, hence, conforms the formation of composite nanoparticle. The value of d-spacing between adjoining lattice fringes in the α-Fe_2O_3 nanoparticle is about 0.25 nm, which indexed to the (110) plane of α-Fe_2O_3. The *d*-spacing between the adjoining lattice fringes of the Co_3O_4 nanoparticle is about 0.147 nm, which corresponds well with the (440) plane of Co_3O_4.

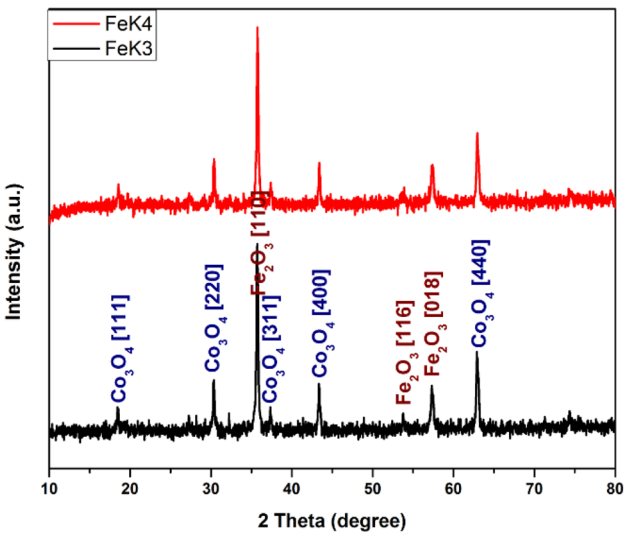

Fig. 1 X-ray diffraction patterns of Fe/Co oxide composite nanoparticles (FeK3 and FeK4)

EDAX

The energy dispersive X-ray spot spectra of the equimolar Fe/Co nanocomposite (sample FeK4) is shown in Fig. 3. The peaks of the spectra confirm the presence of elements Fe, Co, O, Cu and C. The expected peaks for elements Fe, Co and O arise from the composite sample, whereas the peaks corresponding to elements Cu and C arise because carbon-coated copper grid was used in sample preparation for TEM and EDAX analysis.

Raman

The room temperature Raman spectrum of the prepared Fe/Co oxide composite nanoparticles is shown in Fig. 4. As can be seen from Fig. 4, the Raman spectrum of Fe/Co oxide nanocomposites in the range of 100–1600 cm^{-1} show ten obvious peaks located at around 192, 219, 287, 408, 468, 516, 608, 618, 679 and 1296 cm^{-1} corresponding to both α-Fe_2O_3 and Co_3O_4 nanoparticles. The peaks at 192, 468, 516, 608 and 679 cm^{-1} correspond to the five Raman-active modes (F^1_{2g}, E_g, F^2_{2g}, F^3_{2g} and A_{1g}, respectively) of pure Co_3O_4 nanoparticles and the results are consistent with the reported Raman spectrum of crystalline Co_3O_4 (Ramana et al. 2005; Marinkovic-Stanojevic et al. 2007). The Raman mode at 679 cm^{-1} is assigned to the vibrations of the octahedral sites A_{1g}, whereas the F_{2g} and E_g modes are characteristics of coupled vibrations of tetrahedral and octahedral sites (Abu-Zied and Soliman 2009). The phonon lines at wavenumber 219 correspond to A_{1g} mode and at 287, 408 and 618 cm^{-1} represent three E_g modes of α-Fe_2O_3 nanoparticles, respectively. However, for some peaks a maximum shift of around 20 cm^{-1}

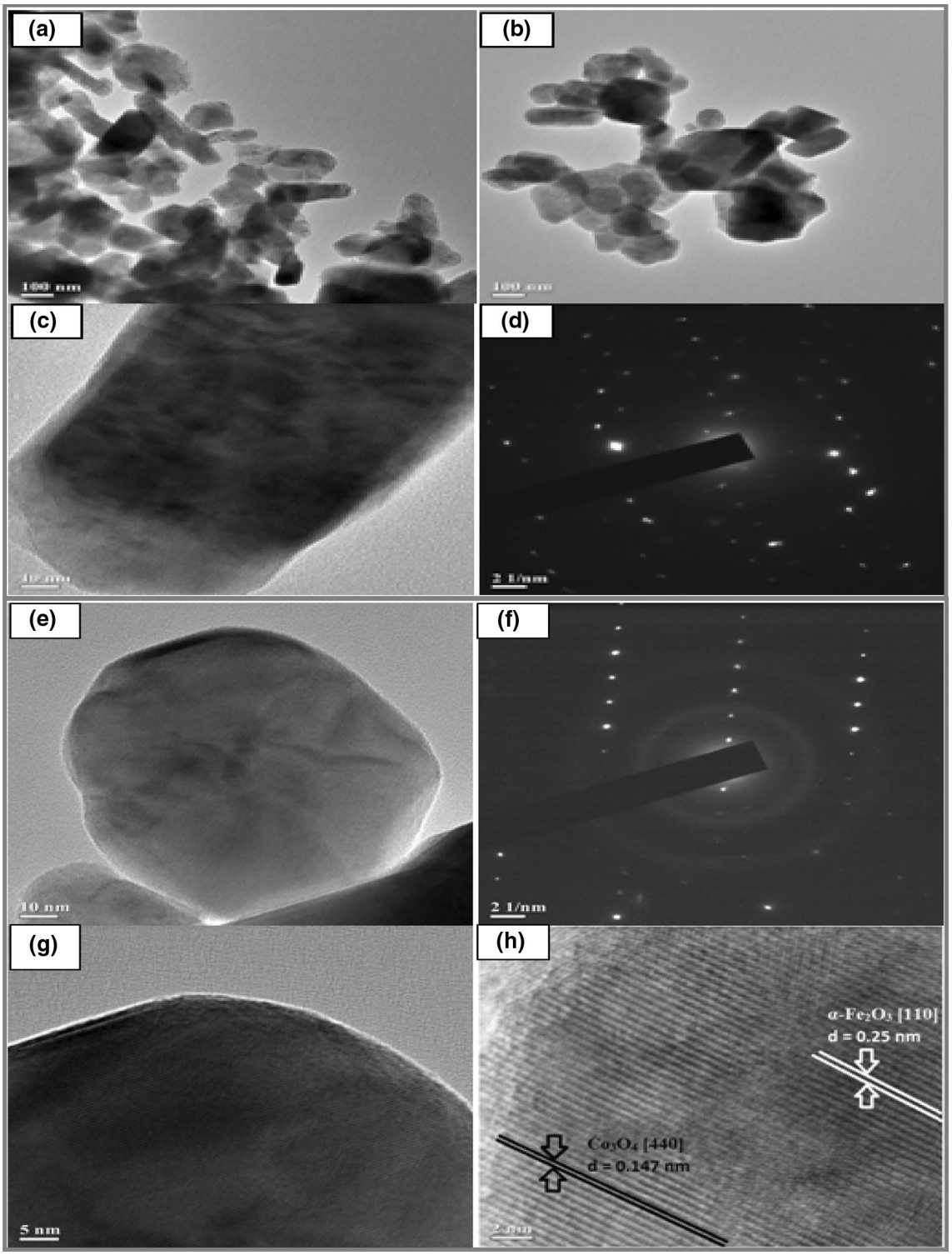

Fig. 2 Transmission electron micrographs of α-Fe_2O_3/Co_3O_4 nanocomposites (sample FeK4)

towards higher wavenumber was observed in the composite sample with equimolar concentration of iron and cobalt which can be assigned to size effects or surface stress/strain. The Raman band at around 1296 cm^{-1} arises due to two magnon scattering originating from the interaction of two magnons formed on antiparallel close spin sites of α-Fe_2O_3 nanoparticles (Chen et al. 2010).

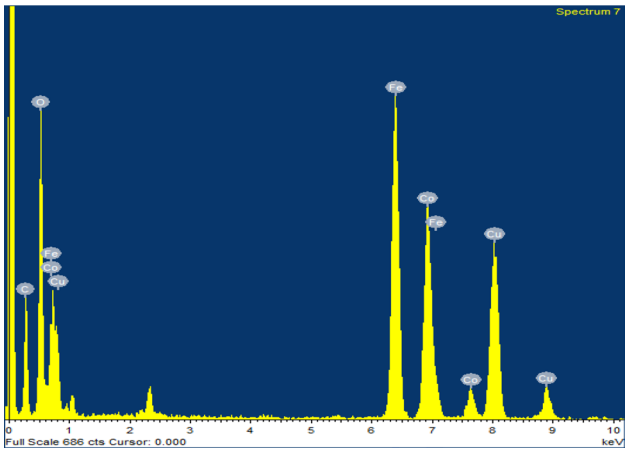

Fig. 3 EDX spot spectra of α-Fe_2O_3/Co_3O_4 nanocomposite (sample FeK4)

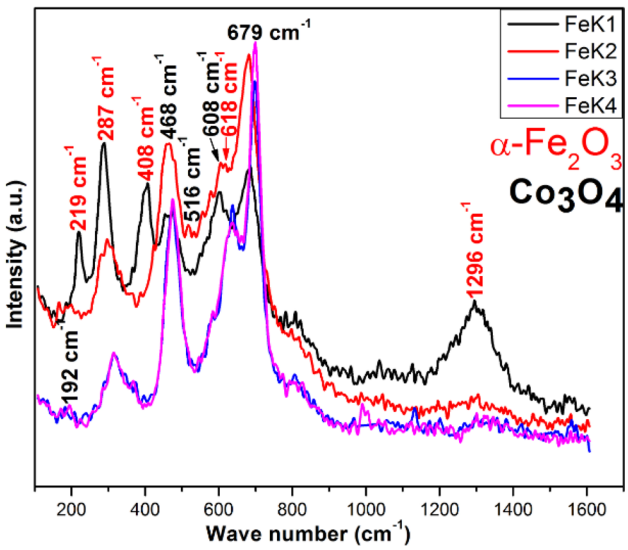

Fig. 4 Raman spectra of Fe/Co oxide composite nanoparticles

Magnetic behaviors

Room temperature magnetization curves of the samples α-Fe_2O_3 and Fe/Co oxide composite nanoparticles are shown in Fig. 5i, and Fig. 5ii shows the room temperature magnetic behavior of Co_3O_4 nanoparticles. All the samples have exhibited strong ferromagnetic characteristics with wide hysteresis loop about the axis. The value of saturation magnetization of the composite samples increases with the increase in cobalt oxide concentrations in the sample. The saturation magnetization value for pure sample of α-Fe_2O_3 was found as 0.24 which has gone up to 82.49 for the FeK4 sample, which is an equimolar nanocomposite of α-Fe_2O_3 and Co_3O_4. The magnetic parameters of α-Fe_2O_3, Co_3O_4

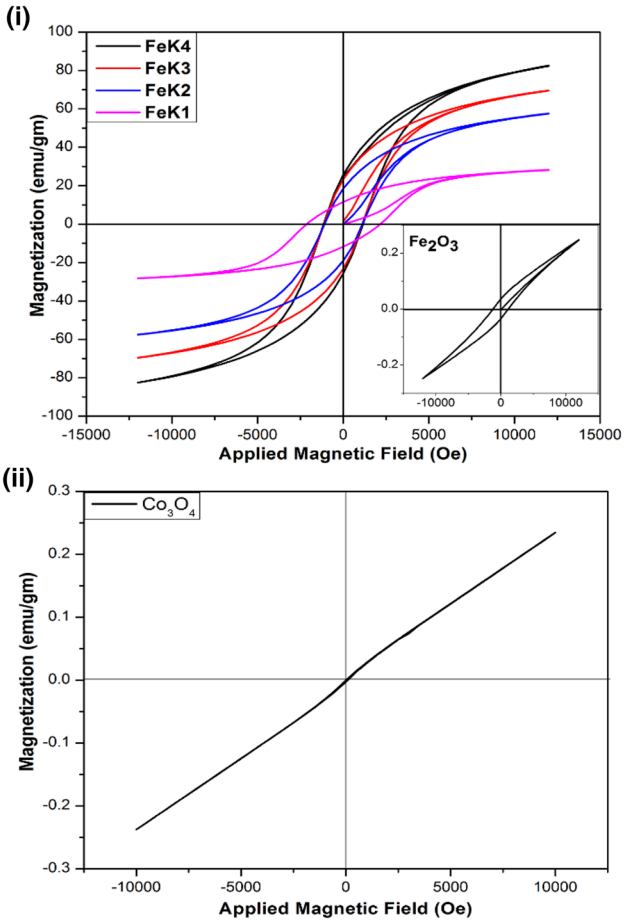

Fig. 5 **i** Magnetization curves of the samples α-Fe_2O_3 and Fe/Co oxide composite nanoparticles. **ii** Magnetization curves of the Co_3O_4 nanoparticles

Table 2 Magnetic parameters of α-Fe_2O_3 and Fe/Co oxide composite nanoparticles

sample code	Coercivity (Gauss)	Retentivity (emu/g)	Magnetization (emu/g)
α-Fe_2O_3	1177.9	0.0350	0.2477
Co_3O_4	35.052	0.0011	0.2360
FeK1	2148.1	11.634	28.244
FeK2	1104.3	18.788	57.571
FeK3	1111.8	23.318	69.567
FeK4	1143.4	25.765	82.493

and Fe/Co oxide composite nanoparticles are summarized in Table 2.

Antibacterial activity

The prepared nanocomposites of Fe/Co oxide are expected to show bactericidal property due to synergistic effect of

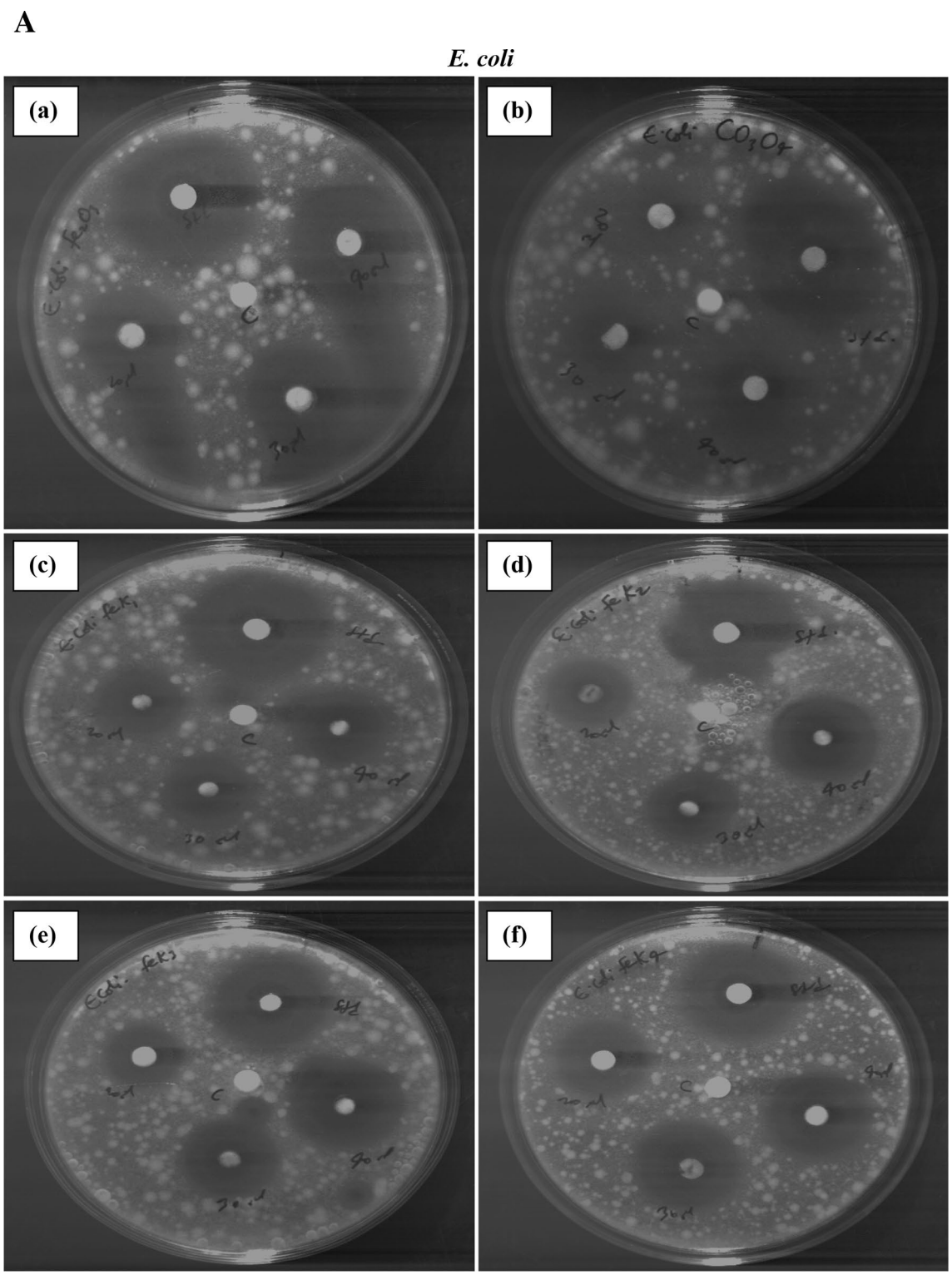

Fig. 6 **A** Zone inhibition of the samples **a** α-Fe_2O_3, **b** Co_3O_4, **c** FeK1, **d** FeK2, **e** FeK3 and **f** FeK4 against bacteria *E. coli*. **B** Zone inhibition of the samples **a** α-Fe_2O_3, **b** Co_3O_4, **c** FeK1, **d** FeK2, **e** FeK3 & **f** FeK4 against bacteria *B. subtilis*. **C** Zone inhibition of the samples **a** α-Fe_2O_3, **b** Co_3O_4, **c** FeK1, **d** FeK2, **e** FeK3 and **f** FeK4 against bacteria *S. aureus*. **D** Zone inhibition of the samples **a** α-Fe_2O_3, **b** Co_3O_4, **c** FeK1, **d** FeK2, **e** FeK3 and **f** FeK4 against bacteria *S. typhi*

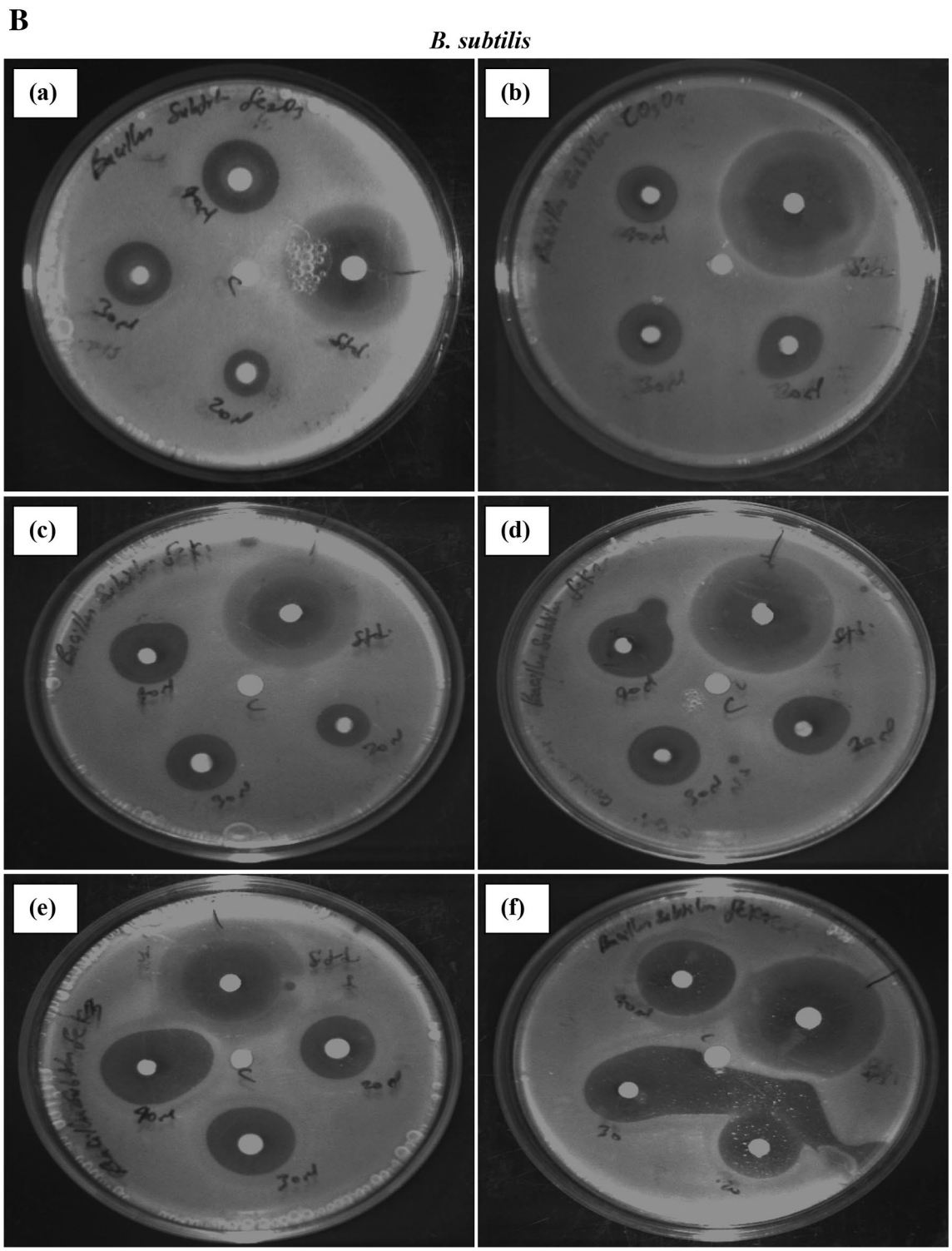

Fig. 6 (continued)

hematite (α-Fe_2O_3) and Co_3O_4 nanocrystals. Hematite nanocrystals have inherent antibacterial properties and the presence of Co_3O_4 nanoparticles in the composite sample likely enhances the bactericidal efficiency of the composite sample perhaps by increasing the overall count of oxygen-free radicals produced as a result of interaction of cytoplasmic water with the composite samples inside bacterial cell. The bactericidal activity of all the prepared samples was

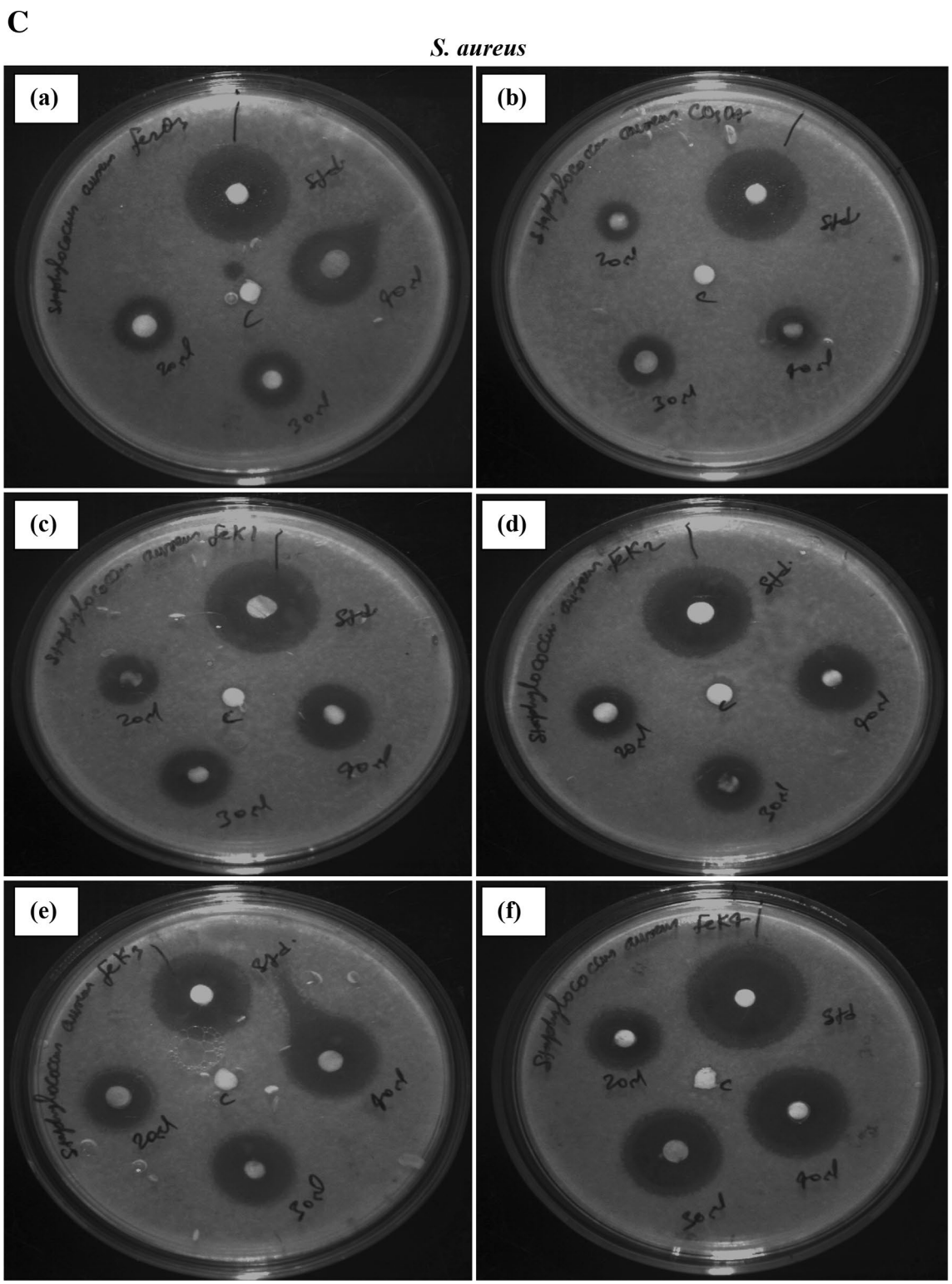

Fig. 6 (continued)

assessed against four pathogenic bacterial strains *B. subtilis*, *S. aureus*, *E.coli* and *S. typhi*.

The results of disc diffusion assay of Fe/Co oxide nanocomposites along with the pure samples of Co_3O_4 and α-Fe_2O_3 against all the tested bacterial strains are shown in

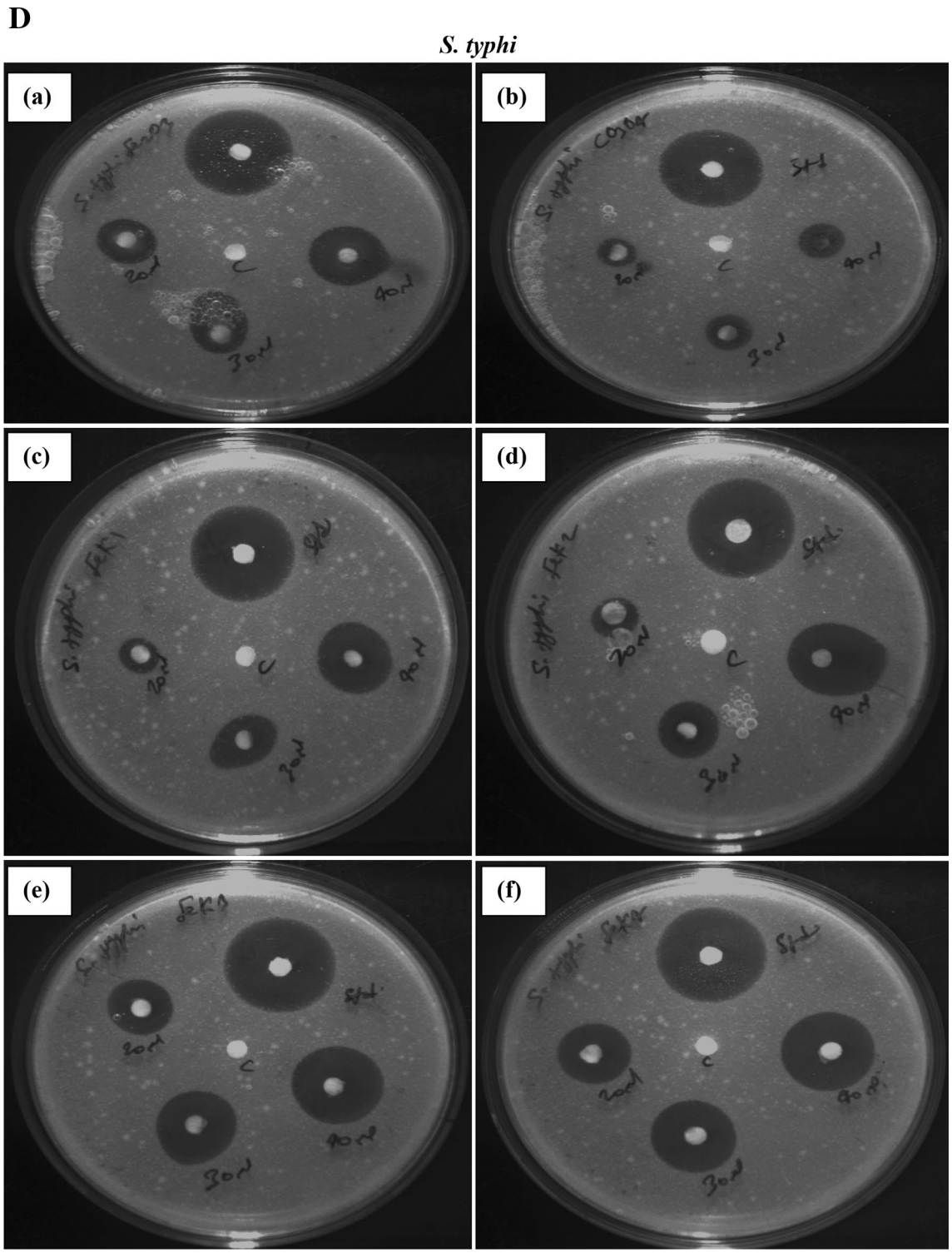

Fig. 6 (continued)

Fig. 6A–D. The motive behind performing Bauer–Kirby disc diffusion assay was to measure the degree of susceptibility of the pathogenic bacteria towards prepared nanomaterials. When the paper disc impregnated with the test sample is placed on the agar plate, at first the disc absorbs water from the agar and then the test sample starts diffusing into agar

Table 3 Inhibition zone size range of the samples α-Fe_2O_3, Co_3O_4, FeK1, FeK2, FeK3 and FeK4 against bacteria *B. subtilis*, *S. aureus*, *E. coli* and *S. typhi*

Conc^n of NPs (in µg)	Zone of inhibition (in mm)						
	Fe_2O_3	Co_3O_4	FeK1	FeK2	FeK3	FeK4	Gentamycin
Bacillus subtilis							
400	11	13	12	16	17	17	32
600	15	13	16	17	19	20	
800	17	13	17	17	20	21	
Staphylococcus aureus							
400	12	10	13	13	14	16	25
600	13	12	15	15	17	22	
800	15	12	17	17	19	24	
Escherichia coli							
400	19	11	18	16	16	18	31
600	20	14	20	18	22	23	
800	21	17	22	24	26	26	
Salmonella typhi							
400	12	0	10	0	14	14	24
600	13	10	12	12	17	17	
800	16	10	16	17	19	19	

surrounding disc. The occurrence or the absence of bacterial growth around the disc in the plate is an indirect measure to assess the antibacterial efficiency of test compounds contrary to exposed bacteria.

There are two observations apparently made from the results of Bauer–Kirby disc diffusion susceptibility test. The first is the diameter of growth inhibition zones produced by the tested samples that is concentration dependent, i.e., for the same sample, higher concentration of the sample (800 µgs) produced larger zones of inhibition. And second is that the diameter of growth inhibition zone increases with increase in cobalt concentration in the composite oxide sample, probably due to the synergistic effect of both hematite and cobalt oxide nanocrystals. Among all the tested samples, the composite samples with higher concentrations of cobalt (FeK3 and FeK4) have shown very efficient bactericidal activity against all the bacterial species with the highest being against *E. coli* and *S. aureus* and the size of inhibition zones produced by them was equivalent to that of commercial antibiotic gentamycin. Among pure samples of α-Fe_2O_3 and Co_3O_4 nanoparticles, α-Fe_2O_3 nanoparticles have produced larger zones of bacterial growth inhibition against all bacteria. The diameters of inhibition zones produced by the tested samples against all bacteria are tabulated in Table 3. Finally, based on the results obtained in the disc diffusion assay, the susceptibility of the bacterial strains against the prepared Fe/Co oxide nanocomposites can be summarized as: *E.coli* > *S. aureus* > *B. subtilis* > *S. typhi*.

Furthermore, to re-assure the antibacterial properties of prepared samples, the bacterial response in the presence of pure as well as composite nanomaterials was recorded by measuring the optical density (OD) of bacterial suspensions at 600 nm at every 6 h interval for 24 h. Growth patterns of bacteria *B. subtilis*, *S. aureus*, *S. typhi* and *E.coli* were obtained by plotting O.D. values against time. Growth patterns of all the selected bacteria were obtained in the presence of varying concentrations of nanoparticles (45, 60, 75, 90 and 120 mg/dl, respectively) in the bacterial growth media. The bacterial culture media without nanoparticles served as control and experienced robust growth of bacteria, while the culture media incubated with nanoparticles experienced reduced bacterial growth.

Figure 7A, B represents the bacterial growth patterns in the presence of Fe/Co oxide nanocomposites, samples FeK1 and FeK4, respectively. Notably, the equimolar nanocomposite of iron and cobalt oxide (sample FeK4) at 120 mg/dl concentration completely diminishes the growth of bacteria *S. aureus* and *E. coli,* while at this concentration; it reduces the growth of *B. subtilis* and *S. typhi* to a large extent. The minimum inhibitory concentration (MIC) values for the sample FeK4 were observed as 90 mg/dl for *B. subtilis*, 75 mg/dl for *S. aureus*, 60 mg/dl for *S. typhi* and 45 mg/dl in case of *E. coli,* respectively. The growth patterns of the selected bacteria in the presence of pure samples of Co_3O_4 and α-Fe_2O_3 nanoparticles are presented in Fig. 7C, D, respectively. The MIC value of the pure samples of Co_3O_4 and α-Fe_2O_3 was found to be 90 mg/dl against *E. coli*. As can be seen from the Fig. 7C, D, both the pure samples exhibited almost similar bactericidal efficiency, with α-Fe_2O_3 being slightly more effective. Finally, based on the growth curve

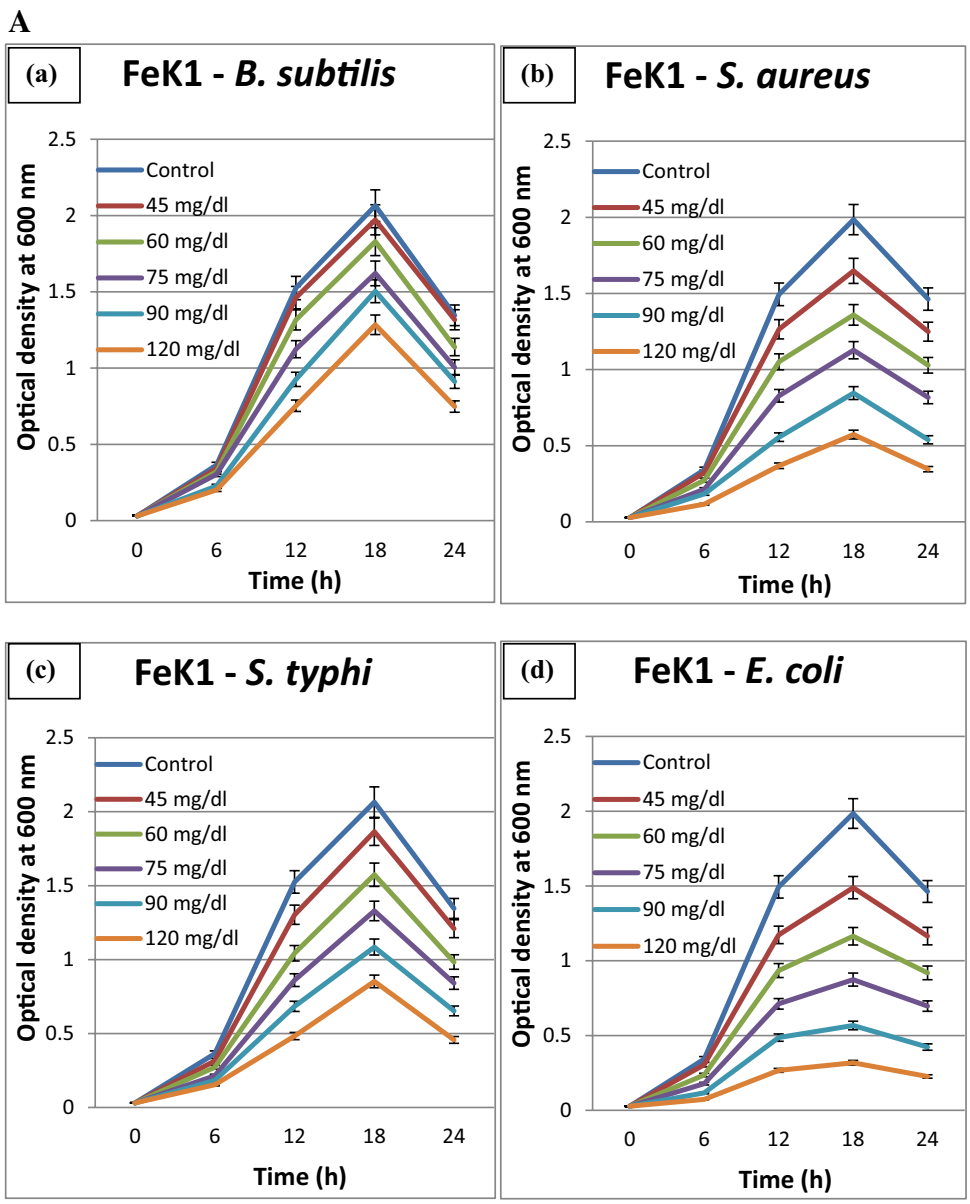

Fig. 7 **A** Growth curves of bacteria **a** *B. subtilis*, **b** *S. aureus*, **c** *S. typhi* and **d** *E. coli* for the sample FeK1. **B** Growth curves of bacteria **a** *B. subtilis*, **b** *S. aureus*, **c** *S. typhi* and **d** *E. coli* for the sample FeK4. **C** Growth curves of bacteria **a** *B. subtilis*, **b** *S. aureus*, **c** *S. typhi* and **d** *E. coli* for the sample Co_3O_4. **D** Growth curves of bacteria **a** *B. subtilis*, **b** *S. aureus*, **c** *S. typhi* and **d** *E. coli* for the sample Fe_2O_3

analysis of the selected bacteria in the presence of prepared samples, the susceptibility of the bacterial strains towards the Fe/Co oxide nanocomposites can be summarized as: *E. coli* > *S. aureus* > *S. typhi* > *B. subtilis*.

Cytotoxicity assay

The biocompatibility and cytotoxic effect of the prepared nanomaterials on MCF7 cells were metabolically quantified through MTT assay. The obtained results were plotted as percentage cell viability versus concentration of nanoparticles and are shown in Fig. 8. As can be inferred from the figure, among all the prepared samples, the minimum percentage cell viability observed was around 82% corresponding to the highest tested concentration (1600 µg/ml) of sample FeK4. More than 80% of the MCF7 cells were viable after 24 h of treatment with all the prepared samples. Based on the obtained results, going by the definition of biocompatibility which requires minimum 80% of cells to be viable after 24 h of treatment with the test material (Zborowski and Chalmers 2007), we can easily say that all our tested samples are biocompatible showing cell viability between 82 and 98% after 24 h of treatment. Again, the cytotoxic effects of the samples were dependent on their

Fig. 7 (continued)

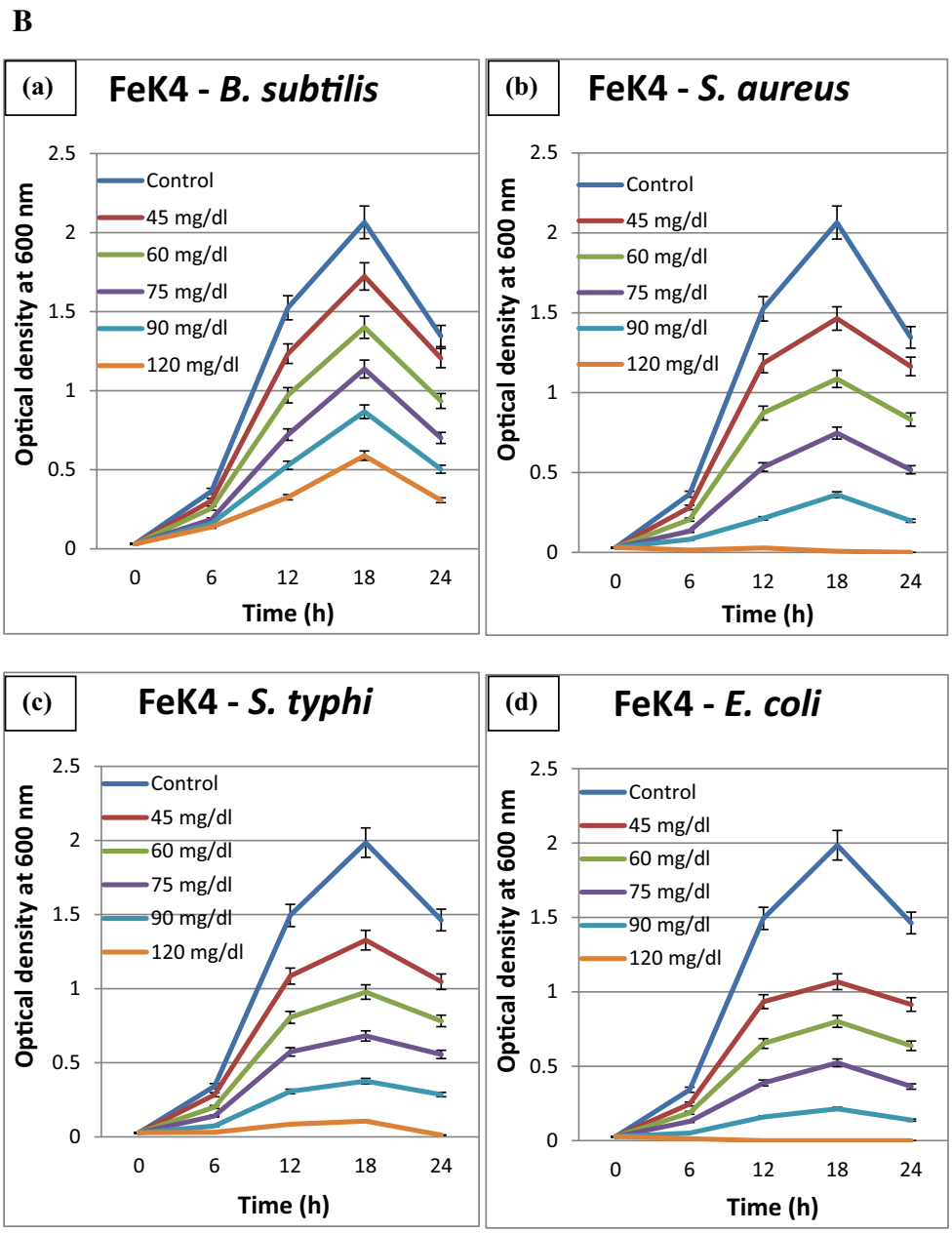

respective doses as well as ionic concentrations. Both the pure samples exhibit almost similar biocompatibility with Co_3O_4 being slightly more toxic than α-Fe_2O_3 nanocrystals. Among nanocomposites, cytotoxicity increases with increase in cobalt oxide content in the sample but still it is well within the permitted limit (< 20%) in case of all the prepared samples.

Conclusions

In the present work, nanocomposites of transition metal oxides (α-Fe_2O_3 and Co_3O_4) were synthesized using co-precipitation method. The X-ray diffraction patterns of the composite samples exhibit characteristic peaks of both hexagonal α-Fe_2O_3 and cubic Co_3O_4. The TEM images show the presence of rod-shaped as well as roughly hexagonal

Fig. 7 (continued)

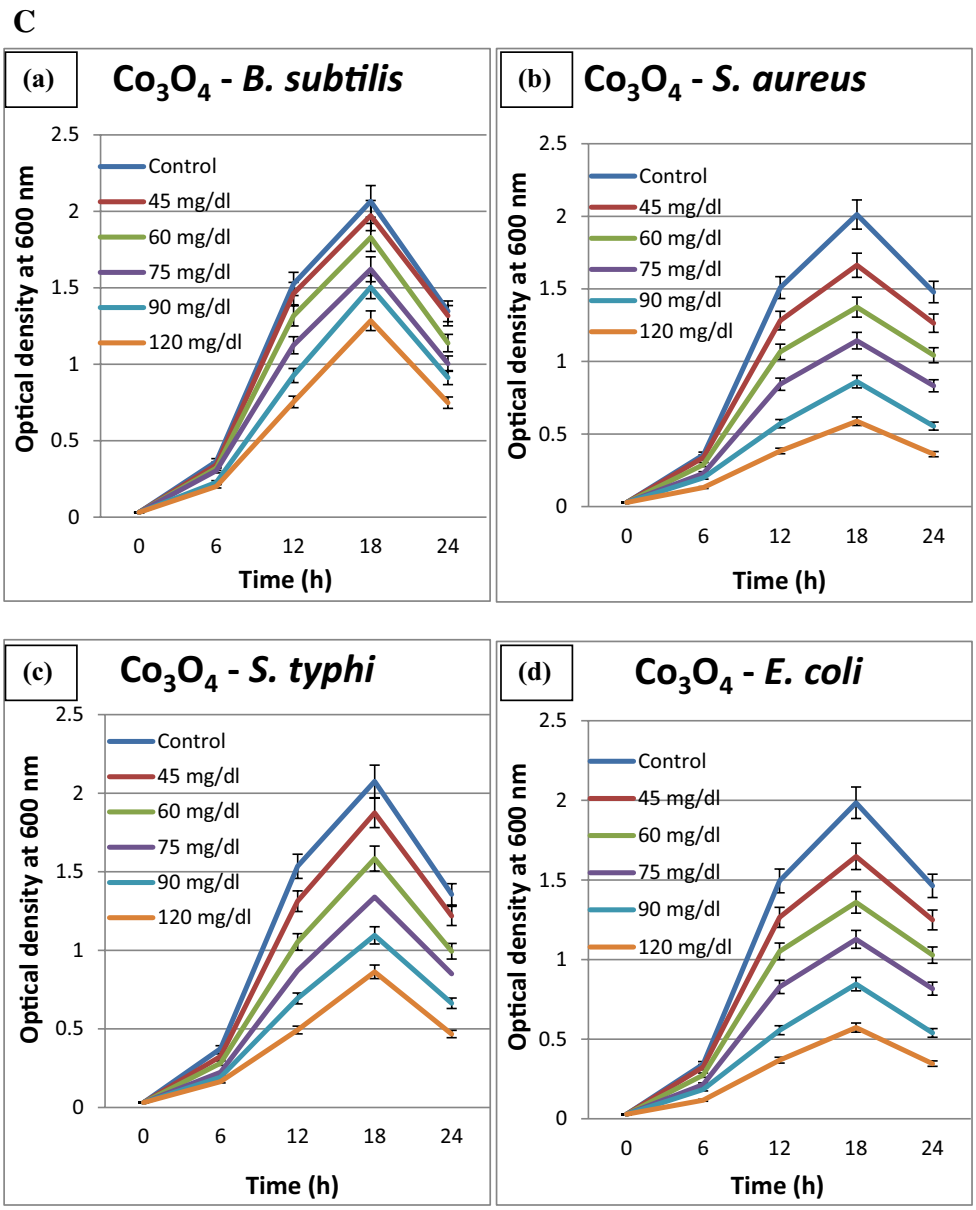

shape nanoparticles. The preferred orientation of α-Fe_2O_3 and Co_3O_4 in the composite sample was [110] and [440] planes, respectively. The value of room temperature saturation magnetization of the composite samples has exhibited an increasing tendency of saturation magnetization value with increase in Co oxide content in the sample. The nanocomposites have exhibited enhanced bactericidal activities against all the bacterial strains used in this study, with respect to the pure samples of α-Fe_2O_3 and Co_3O_4. The sensitivity order of the bacteria against the prepared samples slightly varies with the change in assessment methods (disc diffusion assay and growth curve analysis) because the magnitude of sensitivity of bacteria also depends on local environment such as temperature, pressure and pH, and cell responds differently in different environment. Nevertheless, both the methods have confirmed the efficient bactericidal properties of the prepared nanocomposites and, thus, they can be used as the potent new generation antibiotics to combat contagious diseases caused by bacteria and also they have the potential to combat multi-drug resistant bacteria because of their simultaneous multiple mechanisms of bactericidal action.

Fig. 7 (continued)

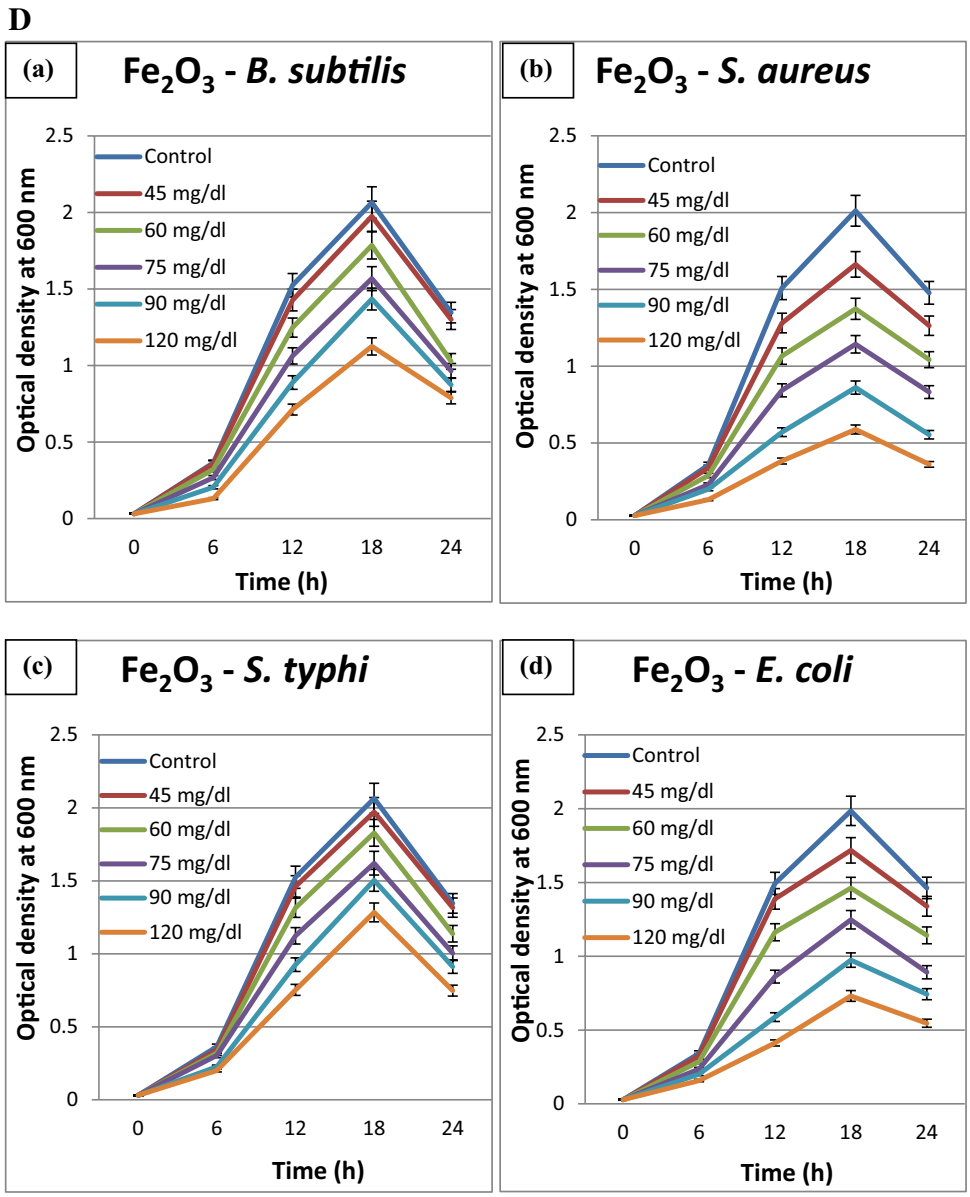

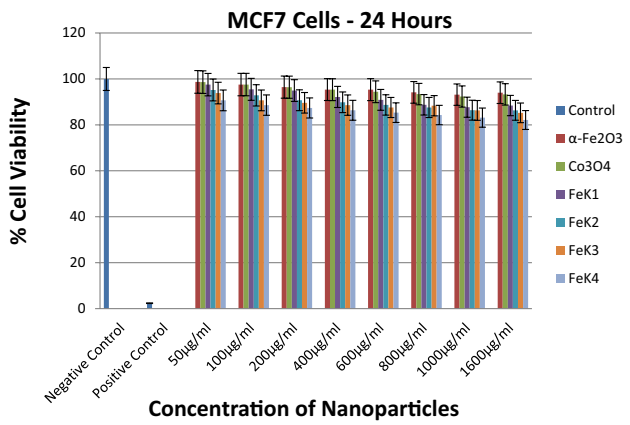

Fig. 8 MTT assay values for samples α-Fe_2O_3, Co_3O_4, FeK1, FeK2, FeK3 and FeK4 against MCF7 cells

Acknowledgements The authors are grateful and would like to thank the people associated with Central Instrumentation Facility, Pondicherry University for allowing us to carry out Raman and VSM studies. Again, we extend our gratefulness and thanks to the TEM unit at Sophisticated Analytical Instrument Facility, North Eastern Hill University-Shillong, for recording TEM images and EDAX of our sample.

Funding This research work did not receive any specific Grant from government, commercial or non-profit funding agencies.

Compliance with ethical standards

Conflict of interest The authors declare that they do not have any conflict of interest.

References

Abu-Zied BM, Soliman SA (2009) Nitrous oxide decomposition over MCO_3–Co_3O_4 (M = Ca, Sr, Ba) catalysts. Catal Lett 132:299–310

Arakha M, Pal S, Samantarrai D, Panigrahi TK, Mallick BC, Pramanik K, Mallick B, Jha S (2015) Antimicrobial activity of iron oxide nanoparticle upon modulation of nanoparticle-bacteria interface. Sci Rep 5:14813. https://doi.org/10.1038/srep14813

Aruguete DM, Bojeong K, Michael FH, Yanjun M, Yingwen C, Andy H, Jie L, Amy P (2013) Antimicrobial nanotechnology: its potential for the effective management of microbial drug resistance and implications for research needs in microbial nanotoxicology. Environ Sci Processes Impacts 15:93–102

Basnet P, Larsen GK, Jadeja RP, Hung YC, Zhao Y (2013) α-Fe_2O_3 nanocolumns and nanorods fabricated by electron beam evaporation for visible light photocatalytic and antimicrobial applications. ACS Appl Mater Interfaces 5(6):2085–2095. https://doi.org/10.1021/am303017c

Bauer AW, Kirby WM, Sherris JC, Turck M (1966) Antibiotic susceptibility testing by a standardized single disk method. Am J Clin Pathol 45(4):493–496

Blecher K, Nasir A, Friedman A (2011) The growing role of nanotechnology in combating infectious disease. Virulence 2:395–401

Brayner R, Dahoumane SA, Yepremian C, Djediat C, Meyer M, Coute A, Fiévet F (2010) ZnO nanoparticles: synthesis, characterization, and ecotoxicological studies. Langmuir 26:6522–6528

Cesar I, Kay A, Gonzalez Martinez JA, Grätzel M (2006) Translucent thin film Fe_2O_3 photoanodes for efficient water splitting by sunlight: nanostructure-directing effect of Si-doping. J Am Chem Soc 128:4582–4583

Chambers HF, DeLeo FR (2009) Waves of resistance: Staphylococcus aureus in the antibiotic era. Nat Rev Microbiol 7:629–641

Chen L, Yang X, Chen J, Liu J, Wu H, Zhan H, Liang C, Wu M (2010) Continuous shape- and spectroscopy-tuning of hematite nanocrystals. Inorg Chem 49:8411–8420

Chen T, Wang R, Xu LQ, Neoh KG, Kang ET (2012) Carboxymethyl chitosan-functionalized magnetic nanoparticles for disruption of biofilms of *Staphylococcus aureus* and *Escherichia coli*. Ind Eng Chem Res 51:13164–13172

Chipara M, Ibrahim E, Yust B, Padilla D, Chipara DM (2015) Nanoparticles and bacteria. J Nanomed Res 2(3):00033. https://doi.org/10.15406/jnmr.2015.02.00033

Dasari TP, Pathakoti K, Hwang HM (2013) Determination of the mechanism of photoinduced toxicity of selected metal oxide nanoparticles (ZnO, CuO, Co_3O_4 and TiO_2) to *E. coli* bacteria. J Environ Sci 25:882–888

Davies J, Davies D (2010) Origins and evolution of antibiotic resistance. Microbiol Mol Biol Rev 74:417–433

Denizot F, Lang R (1986) Rapid colorimetric assay for cell growth and survival: modifications to the tetrazolium dye procedure giving improved sensitivity and reliability. J Immunol Methods 89(2):271–277

Foster HA, Ditta IB, Varghese S, Steele A (2011) Photocatalytic disinfection using titanium dioxide: spectrum and mechanism of antimicrobial activity. Appl Microbiol Biotechnol 90:1847–1868

Fu G, Vary PS, Lin CT (2005) Anatase TiO_2 nanocomposites for antimicrobial coatings. J Phys Chem B 109:8889–8898

Ghosh T, Dash SK, Chakraborty P, Guha A, Kawaguchi K, Roy S, Chattopadhyay T, Das D (2014) Preparation of antiferromagnetic Co_3O_4 nanoparticles from two different precursors by pyrolytic method: in vitro antimicrobial activity. RSC Adv 4:15022–15029

Hajipour MJ, Fromm KM, Ashkarran AA, Jimenez de Aberasturi D, Larramendi IRD, Rojo T, Serpooshan V, Parak WJ, Mahmoudi M (2012) Antibacterial properties of nanoparticles. Trends Biotechnol 30:499–511

Hood MI, Skaar EP (2012) Nutritional immunity: transition metals at the pathogen–host interface. Nat Rev Microbiol 10:525–537

Huh AJ, Kwon YJ (2011) "Nanoantibiotics": a new paradigm for treating infectious diseases using nanomaterials in the antibiotics resistant era. J Control Release 156:128–145

Jayaraman R (2009) Antibiotic resistance: an overview of mechanisms and a paradigm shift. Curr Sci 96:1475–1484

Khan S, Ansari AA, Khan AA, Ahmad R, Al-Obaid O, Al-Kattan W (2015) In vitro evaluation of anticancer and antibacterial activities of cobalt oxide nanoparticles. J Biol Inorg Chem 20(8):1319–1326. https://doi.org/10.1007/s00775-015-1310-2

Kohanski MA, Dwyer DJ, Hayete B, Lawrence CA, Collins JJ (2007) A common mechanism of cellular death induced by bactericidal antibiotics. Cell 130:797–810

Kong H, Song J, Jang J (2010) One-step fabrication of magnetic γ-Fe_2O_3/polyrhodanine nanoparticles using in situ chemical oxidation polymerization and their antibacterial properties. Chem Commun 46:6735–6737

Levy SB, Marshall B (2004) Antibacterial resistance worldwide: causes, challenges and responses. Nat Med 10:S122–S129. https://doi.org/10.1038/nm1145

Liu J, Aruguete DM, Murayama M, Hochella MF (2009) Influence of size and aggregation on the reactivity of an environmentally and industrially relevant nanomaterial (PbS). Environ Sci Technol 43:8178–8183

Makhluf S, Dror R, Nitzan Y, Abramovich Y, Jelinek R, Gedanken A (2005) Microwave-assisted synthesis of nanocrystalline MgO and Its use as a bacteriocide. Adv Funct Mater 15:1708–1715

Marinkovic-Stanojevic ZV, Romcevic N, Stojanovic BD (2007) Spectroscopic study of spinel $ZnCr_2O_4$ obtained from mechanically activated ZnO–Cr_2O_3 mixtures. J Eur Ceram Soc 27:903–907

Moritz M, Geszke-Moritz M (2013) The newest achievements in synthesis, immobilization and practical applications of antibacterial nanoparticles. Chem Eng J 228:596–613

Mosmann T (1983) Rapid colorimetric assay for cellular growth and survival: application to proliferation and cytotoxicity assays. J Immunol Methods 65(1–2):55–63

Nor YA, Zhou L, Meka AK, Xu C, Niu Y, Zhang H, Mitter N, Mahony D, Yu C (2016) Engineering iron oxide hollow nanospheres to enhance antimicrobial property: understanding the cytotoxic origin in organic rich environment. Adv Funct Mater 26:5408–5418

Nussbaum FV, Brands M, Hinzen B, Weigand S, Häbich D (2006) Antibacterial natural products in medicinal chemistry—exodus or revival? Angew Chem Int Ed 45:5072–5129

Pareta RA, Taylor E, Webster TJ (2008) Increased osteoblast density in the presence of novel calcium phosphate coated magnetic nanoparticles. Nanotechnology 19:265101. https://doi.org/10.1088/0957-4484/19/26/265101

Parham S, Wicaksono DHB, Bagherbaigi S, Lee SL, Nur H (2016) Antimicrobial treatment of different metal oxide nanoparticles: a critical review. J Chin Chem Soc 63:385–393

Pelgrift RY, Friedman AJ (2013) Nanotechnology as a therapeutic tool to combat microbial resistance. Adv Drug Deliv Rev 65:1803–1815

Rafi MM, Ahmed KSZ, Nazeer KP, Kumar DS, Thamilselvan M (2015) Synthesis, characterization and magnetic properties of hematite (α-Fe_2O_3) nanoparticles on polysaccharide templates and their antibacterial activity. Appl Nanosci 5:515–520. https://doi.org/10.1007/s13204-014-0344-z

Ramana CV, Massot M, Julien CM (2005) XPS and Raman spectroscopic characterization of $LiMn_2O_4$ spinels. Surf Interface Anal 37:412–416

Rudramurthy GR, Swamy MK, Sinniah UR, Ghasemzadeh A (2016) Nanoparticles: alternatives against drug-resistant pathogenic

microbes. Molecules 21:836. https://doi.org/10.3390/molecules21070836
Rufus A, Sreeju N, Philip D (2016) Synthesis of biogenic hematite (α-Fe_2O_3) nanoparticles for antibacterial and nanofluid applications. RSC Adv 6:94206–94217. https://doi.org/10.1039/C6RA20240C
Sharma P, Rana DS, Ahmad U, Kumar R, Negi K, Chauhan MS, Chauhan S (2016) Iron oxide nanocubes for photocatalytic degradation and antimicrobial applications. Nanosci Nanotechnol Lett 8:1014–1019
Stankic S, Suman S, Haque F, Vidic J (2016) Pure and multi metal oxide nanoparticles: synthesis, antibacterial and cytotoxic properties. J Nanobiotechnol 14:73. https://doi.org/10.1186/s12951-016-0225-6
Touati D (2000) Iron and oxidative stress in bacteria. Arch Biochem Biophys 373:1–6
Tran N, Mir A, Mallik D, Sinha A, Nayar S, Webster TJ (2010) Bactericidal effect of iron oxide nanoparticles on *Staphylococcus aureus*. Int J Nanomed 5:277–283
Wan H, Williams RL, Doherty PJ, Williams DF (1994) The cytotoxicity evaluation of Kevlar and silicon carbide by MTT assay. J Mater Sci 5(6–7):441–445
Wang Z, Lee YH, Wu B, Horst A, Kang Y, Tang YJ, Chen DR (2010) Anti-microbial activities of aerosolized transition metal oxide nanoparticles. Chemosphere 80:525–529
Weinberg ED (1999) Iron loading and disease surveillance. Emerg Infect Dis 5:346–352
Xia Y (2008) Nanomaterials at work in biomedical research. Nat Mater 7:758–760
Zborowski M, Chalmers JJ (2007) Magnetic cell separation, 1st edn. Elsevier, Amsterdam
Zhang H, Chen B, Banfield JF (2010) Particle size and pH effects on nanoparticle dissolution. J Phys Chem C 114:14876–14884
Zhang Q, Lambert G, Liao D, Kim H, Robin K, Tung CK, Pourmand N, Austin RH (2011) Acceleration of emergence of bacterial antibiotic resistance in connected microenvironments. Science 333(6050):1764–1767. https://doi.org/10.1126/science.1208747